AMPTIAC

70258

ORNL-4162
UC-25 – Metals, Ceramics, and Materials

MECHANICAL BEHAVIOR OF CHEMICALLY VAPOR DEPOSITED TUNGSTEN AT ELEVATED TEMPERATURES

H. E. McCoy, Jr.
J. O. Stiegler

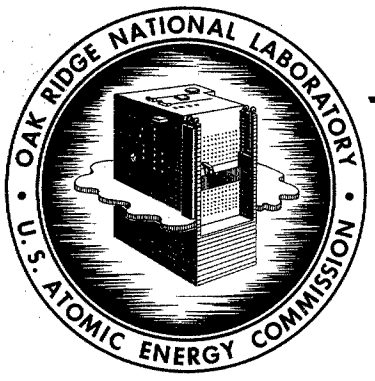

OAK RIDGE NATIONAL LABORATORY
operated by
UNION CARBIDE CORPORATION
for the
U.S. ATOMIC ENERGY COMMISSION

Printed in the United States of America. Available from Clearinghouse for Federal Scientific and Technical Information, National Bureau of Standards, U.S. Department of Commerce, Springfield, Virginia 22151
Price: Printed Copy $3.00; Microfiche $0.65

ORNL-4162

Contract No. W-7405-eng-26

METALS AND CERAMICS DIVISION

MECHANICAL BEHAVIOR OF CHEMICALLY VAPOR DEPOSITED TUNGSTEN AT ELEVATED TEMPERATURES

H. E. McCoy, Jr. J. O. Stiegler

Paper for Conference on Chemical Vapor Deposition of Refractory Metals, Alloys and Compounds, Gatlinburg, Tennessee, September 12–13, 1967

SEPTEMBER 1967

OAK RIDGE NATIONAL LABORATORY
Oak Ridge, Tennessee
operated by
UNION CARBIDE CORPORATION
for the
U.S. ATOMIC ENERGY COMMISSION

CONTENTS

MECHANICAL BEHAVIOR OF CHEMICALLY VAPOR DEPOSITED TUNGSTEN AT ELEVATED TEMPERATURES

H. E. McCoy, Jr. J. O. Stiegler

ABSTRACT

Many applications of chemically vapor deposited (CVD) tungsten require that the material be stressed at elevated temperatures. We have run creep-rupture tests at 1650 and 2200°C to evaluate the mechanical behavior of this material, and the properties are compared with those of a typical heat of powder metallurgy (PM) tungsten. At 1650°C the CVD product has low fracture strains (approx 5%) and a lower minimum creep rate. At high stresses the rupture life is shorter than that of the PM material; at low stresses the rupture lives are about equivalent. At 2200°C the minimum creep rate is higher and the rupture life lower for the CVD product.

Two microstructural features of importance were noted in the CVD tungsten: (1) the formation and growth of voids and (2) the columnar nature of the grains. Fractographic techniques were used to study void nucleation and growth in the material. Nucleation appears to be spontaneous as the material is heated to elevated temperatures, indicating the presence of an impurity having a high vapor pressure. The growth appears to occur almost entirely by the stress-induced diffusion of vacancies into the void. At 2200°C under stress the voids reach such a large size that they comprise about 10% of the test specimen. The columnar grain structure of the material is important because it is very difficult to get extensive grain-boundary sliding and rotation in this type of structure.

We have rationalized the creep behavior of this material on the basis of the effects that both the void growth and the columnar grain structure have on the individual deformation processes that sum to give the overall creep behavior.

INTRODUCTION

Chemical vapor deposition (CVD) is now recognized as an attractive way of obtaining complex tungsten shapes without subsequent fabrication as well as a means of obtaining high-purity stock for further fabrication.

The production process generally involves the hydrogen reduction of WF_6 to deposit tungsten on a heated substrate.[1] It has been shown that, after suitable heat treatment, the low-temperature mechanical properties of the CVD tungsten are comparable with those of tungsten produced by conventional methods.[2] The excellent resistance of tungsten produced by this process to grain growth at elevated temperatures has also been demonstrated.[3–5] However, voids have been observed when this material is annealed at elevated temperatures, particularly when a stress is applied.[3,5,6] Taylor and Boone[6] found that the tensile strength and fracture ductility of the CVD material were less than the respective values for powder metallurgy (PM) tungsten, but the creep properties of this material have not been evaluated.

In the present study we evaluated the creep-rupture properties of several lots of CVD tungsten at 1650 and 2200°C. We shall compare the results of these tests with those of similar tests on a heat of PM tungsten. Since the properties of the two materials differed considerably, we performed extensive optical and electron microscopy in an effort to ascertain the reasons for the differences. Although numerous unanswered questions remain, we were able to propose a qualitative explanation for the creep-rupture behavior of CVD tungsten.

---

[1]R. L. Heestand, J. I. Federer, and C. F. Leitten, Jr., Preparation and Evaluation of Vapor Deposited Tungsten, ORNL-3662 (August 1964).

[2]A. C. Schaffhauser, "Low-Temperature Ductility and Strength of Thermochemically Deposited Tungsten and Effects of Heat Treatment," pp. 261–276 in Summary of the Eleventh Refractory Composites Working Group Meeting, AFML-TR-66-179 (July 1966).

[3]A. C. Schaffhauser and R. L. Heestand, "Effect of Fluorine Impurities on the Grain Stability of Thermochemically Deposited Tungsten," pp. 204–211 in 1966 IEEE Conference Record of the Thermionic Conversion Specialist Conference, Institute of Electrical and Electronics Engineers, New York, 1966.

[4]A. F. Weinberg, J. R. Lindgren, N. B. Elsner, and R. G. Mills, Grain Growth Characteristics of Vapor-Deposited Tungsten at Temperatures up to 2500°C, GA-6231 (1965).

[5]H. E. McCoy, Creep-Rupture Properties of Tungsten and Tungsten-Base Alloys, ORNL-3992 (1966).

[6]J. L. Taylor and D. H. Boone, J. Less-Common Metals 6, 157 (1964).

EXPERIMENTAL DETAILS

Test Materials

The PM sheet used in this study was obtained under a Bureau of Naval Weapons Contract and the fabrication details are covered in the final report on this contract.[7] It was fabricated by the PM technique and was rolled to a final thickness of 0.060 in. The final treatment was a 5-min anneal at 1150°C. The high purity of this material is illustrated by the results of chemical analyses shown in Tables 1 and 2.

The CVD material was produced by the hydrogen reduction of WF_6 on a heated substrate. The details of the deposition process have been described previously.[1] The material was deposited as a box about 2 by 2 in. in cross section and 20 in. long; the thickness varied from 0.050 to 0.060 in. It was deposited on the inside of a mandrel — copper for the "H" series; molybdenum for the "P" series. The mandrel was removed by chemical etching, and test specimens were made from the sides of the box. Chemical data are given for several heats in Tables 1 and 2.

---

[7]G. C. Bodine, Tungsten Sheet Rolling Program — Final Report Covering Period 1 June 1960 to 1 March 1963, Fansteel Metallurgical Corporation, under Contract No. NDW-60-0621-C (March 1, 1963).

Table 1. Chemical Composition of Test Materials

Lot Number	Chemical Content (wt %)				F (ppm)
	O	N	C	H	
Powder metallurgy	0.0029	< 0.0005	< 0.001	0.0004	5
CVD, PW-3	0.011	< 0.0005	0.003	0.0004	21
CVD, PW-19	0.014	0.0009	0.002	0.0005	23
CVD, PW-20	< 0.0005	< 0.0005	0.003	0.0001	16
CVD, PW-23	0.0067	< 0.0005	0.001	0.0002	22
CVD, PW-24	0.022	0.0014	0.004	0.0002	21
CVD, PW-18	0.0010	< 0.0005	< 0.001	0.0002	9,5
CVD, PW-69	0.0005	< 0.0005	0.0006	0.0002	25,28
CVD, H-16	0.0064	< 0.0005	0.002	0.0005	14

Table 2. Semiquantitative Chemical Analysis in Parts Per Million (Weight)

Element	PM	PW-3	H-16	PW-18	PW-20
Al		0.2	0.4	0.1	0.3
B	0.06	0.06	0.06	0.7	0.7
Ca	2	0.2	0.2	< 0.1	0.7
Cd	< 0.1	< 0.1	< 0.1	6	< 0.1
Co		0.03		< 0.1	< 0.1
Cr	3	3	1	0.3	1
Cu	0.3	1	0.03	< 0.1	< 0.1
Fe	3	9	3	2	3
K	0.6	2	0.6	< 0.1	< 0.1
Mg	0.1	< 0.1	0.5	0.1	0.1
Mn	0.1	0.1	0.03	0.1	0.03
Mo	20	6	6	0.3	0.3
Ni	1			0.1	0.2
S	3	10	10	< 0.1	< 0.1
Ta	3	3	3		
V	0.1	0.03	0.03	< 0.1	< 0.1

Test Specimens

A small sheet test specimen with a gage section 1.5 by 0.25 in. and an overall length of 3.5 in. was used. There were small holes near each end for pinning the specimen to the extension rods. The PM tungsten specimens were made by grinding. The CVD tungsten was too fragile for grinding and the specimens were made by electrodischarge machining. A tool was made for the Elox machine which utilized simple brass shapes.[5] The tool was inexpensive and could be rebuilt easily. About 0.002 in. was removed from the machined surfaces by abrasion with diamond paste to remove small intergranular cracks that were formed by the electrodischarge machining. The as-deposited surfaces were lapped in some instances, but this did not seem to have any effect on the high-temperature properties.

Testing Methods

All of the tests were run in a Brew Creep Testing Apparatus, Model No. 1064, having a tungsten mesh heating element. The vacuum system was cold trapped and was capable of maintaining a pressure of 1×10^{-7} torr at a test temperature of 2200°C. The temperature was automatically controlled using a total radiation pyrometer which was sighted on the test specimen and a controller which adjusted the power to the furnace. This control system was stated to have a control accuracy of ±3°C. The temperature could also be read by an optical pyrometer through a sight port in the front of the test chamber. The strain was measured by a dial gage which indicated the motion of the pull rod.

Test specimens were normally built into the test equipment, pumped for 2 hr, heated to about 600°C and pumped for 12 hr, heated to the test temperature in about 4 hr, and loaded.

Several specimens were analyzed for interstitials after testing. No evidence of contamination was noted except in cases where the pressure was known to have increased during the test. Data from tests where leaks were known to have developed have not been considered.

At the time the specimens fractured, the lower pull rod dropped and caused a temporary pressure rise that caused the power to the furnace to be cut off. Since the specimens were heated by radiation, the cooling rate was high enough that the structures observed subsequently were typical of the deformed state.

Fractographic Techniques

Tungsten fractures in a brittle, intergranular manner at low temperatures, and voids formed at elevated temperatures can be exposed without distortion by snapping the specimens at room temperature. The fracture surfaces were replicated directly with carbon and shadowed with platinum. Replicas were taken from the creep-fracture surfaces and from surfaces below the original fracture surface that were exposed by fracturing at room temperature. The replicas were examined in the electron microscope to determine details about the voids such as size, number, geometry, and location.

EXPERIMENTAL OBSERVATIONS

The creep-rupture properties of several lots of CVD tungsten are compared with those for PM tungsten in Fig. 1. At 1650°C the rupture life of the CVD tungsten is generally less at higher stresses (e.g., 6000 psi) and equivalent at lower stresses. Lot PW-20 is somewhat anomalous in that its rupture life is greater than that of PM tungsten. At 2200°C the CVD material has a shorter rupture life except for the PW-3 specimen tested at the lowest stress.

Figure 2 compares the minimum creep rates of PM and CVD tungsten. At 1650°C the CVD material exhibits a lower creep rate and at 2200°C the opposite is noted.

The fracture strains for the CVD and PM materials are compared in Fig. 3. At 1650°C the CVD material exhibited strains of about 5% with only two notable exceptions — lot PW-18 with 13.2% and H-16 with 21.0%. The two exceptions are quite important and will be discussed later. At 2200°C grain growth occurs quite rapidly in the PM tungsten and this probably accounts for the decrease in ductility with increasing rupture

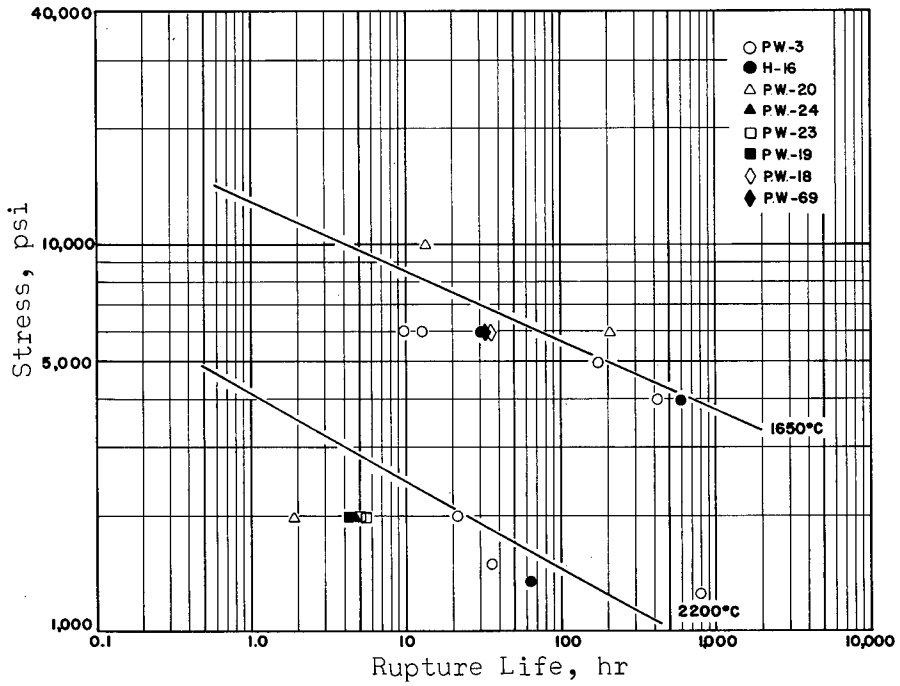

Fig. 1. Comparison of the Creep-Rupture Properties of CVD and PM Tungsten.

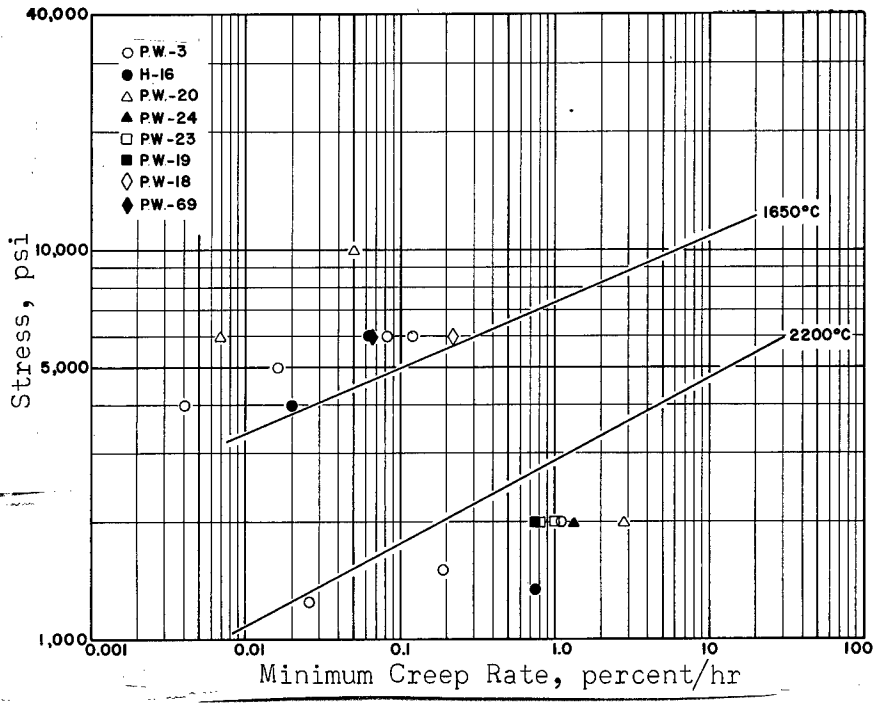

Fig. 2. Comparison of Minimum Creep Rates of CVD and PM Tungsten.

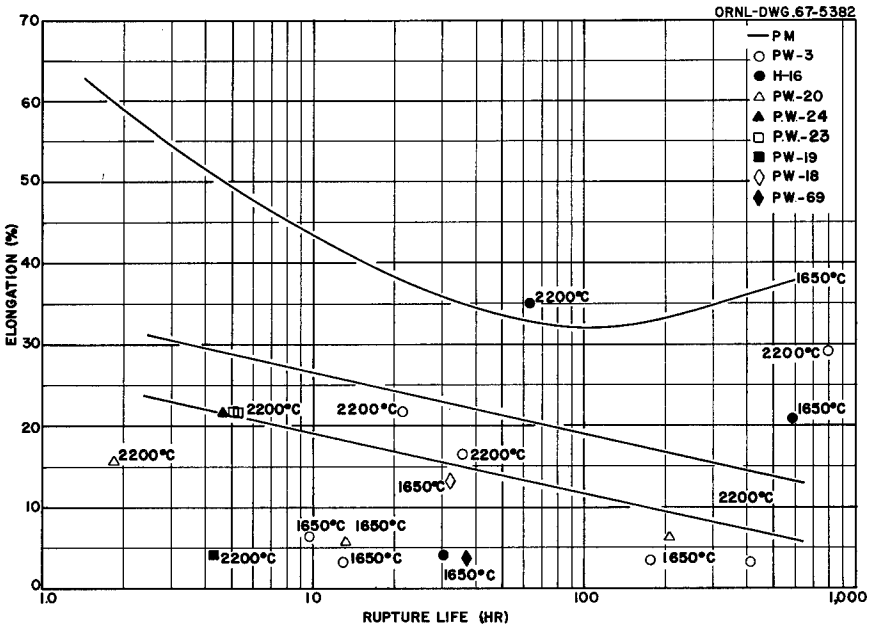

Fig. 3. Comparison of Fracture Ductilities of CVD and PM Tungsten.

life. The CVD tungsten generally exhibits fracture strains in the range of 15 to 25% at 2200°C. Again there are two exceptions – lot PW-19 at 4.2% and PW-3 at 29.2%.

A detailed study has been made of the intergranular void formation in PM tungsten and these findings have been reported previously.[8] However, we shall show some typical micrographs for the purpose of making comparisons between the PM and CVD materials. Figure 4 shows the fracture of a PM specimen tested at 6000 psi and 1650°C. The failure is obviously due to the linking of intergranular cracks. The fractograph shown in Fig. 5, from a region 10 mm below the high-temperature fracture surface, shows these cracks in an early stage of development. These

[8]J. O. Stiegler, K. Farrell, B.T.M. Loh, and H. E. McCoy, "Nature of Creep Cavities in Tungsten," submitted to Transactions of the American Society for Metals.

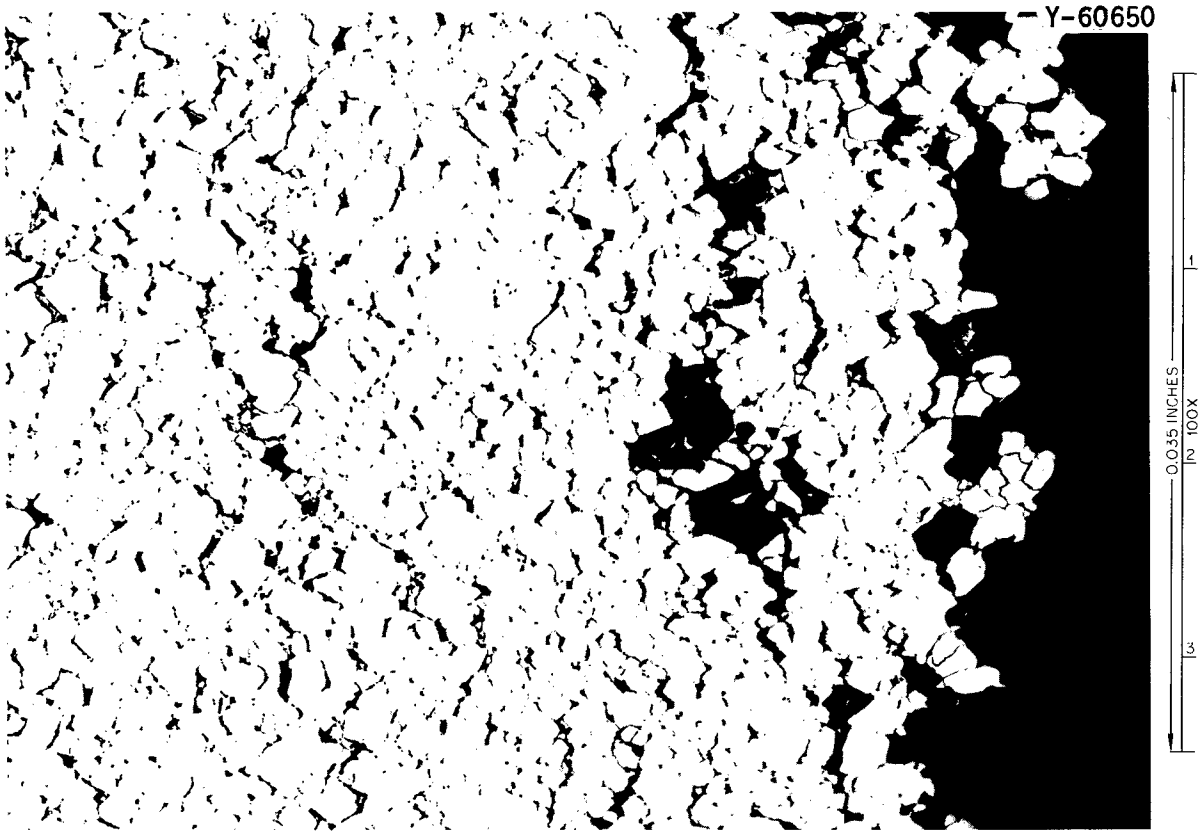

Fig. 4. Photomicrograph of PM Tungsten Sheet Tested at 6000 psi and 1650°C. Rupture occurred at 135 hr and 31.2% strain. As polished.

Fig. 5. Fractograph of a PM Tungsten Specimen Tested at 1650°C and 7000 psi. 11,250×.

cracks originate as intergranular voids that are located quite randomly and are irregular in shape. There is considerable evidence of preferential growth and linking in particular directions. The larger irregularly shaped voids would appear as intergranular cracks when viewed perpendicularly to the plane of Fig. 5.

Figure 6 shows the microstructure of PM tungsten after testing at 1500 psi and 2200°C. Features of importance are the extensive grain

Fig. 6. Photomicrograph of PM Tungsten Tested at 1500 psi and 2200°C. Rupture occurred at 42.1 hr and 16.6% strain. Etchant: 50 parts NH_4OH and 50 parts H_2O_2.

growth and the formation of intergranular voids. The fractograph in Fig. 7 defines the nature of the intergranular voids more accurately. The voids have well-defined shapes and the details of the crystallography are discussed elsewhere.[9]

The CVD tungsten is characterized by large columnar grains which are oriented in the thickness dimension of the deposited sheet. A layer of small grains forms at the substrate surface where the deposit begins. A cross-sectional view of a CVD tungsten sheet is shown in Fig. 8a. This particular sheet is atypical in that the gas supply was interrupted and a laminate formed near the center of the sheet. A view of the sheet parallel to the surface is shown in Fig. 8b. The microstructure in this plane gives the appearance of an equiaxial grain structure. The test

[9]K. Farrell, B.T.M. Loh, and J. O. Stiegler, "Morphologies of Bubbles and Voids in Tungsten," submitted to Transactions of the American Society for Metals.

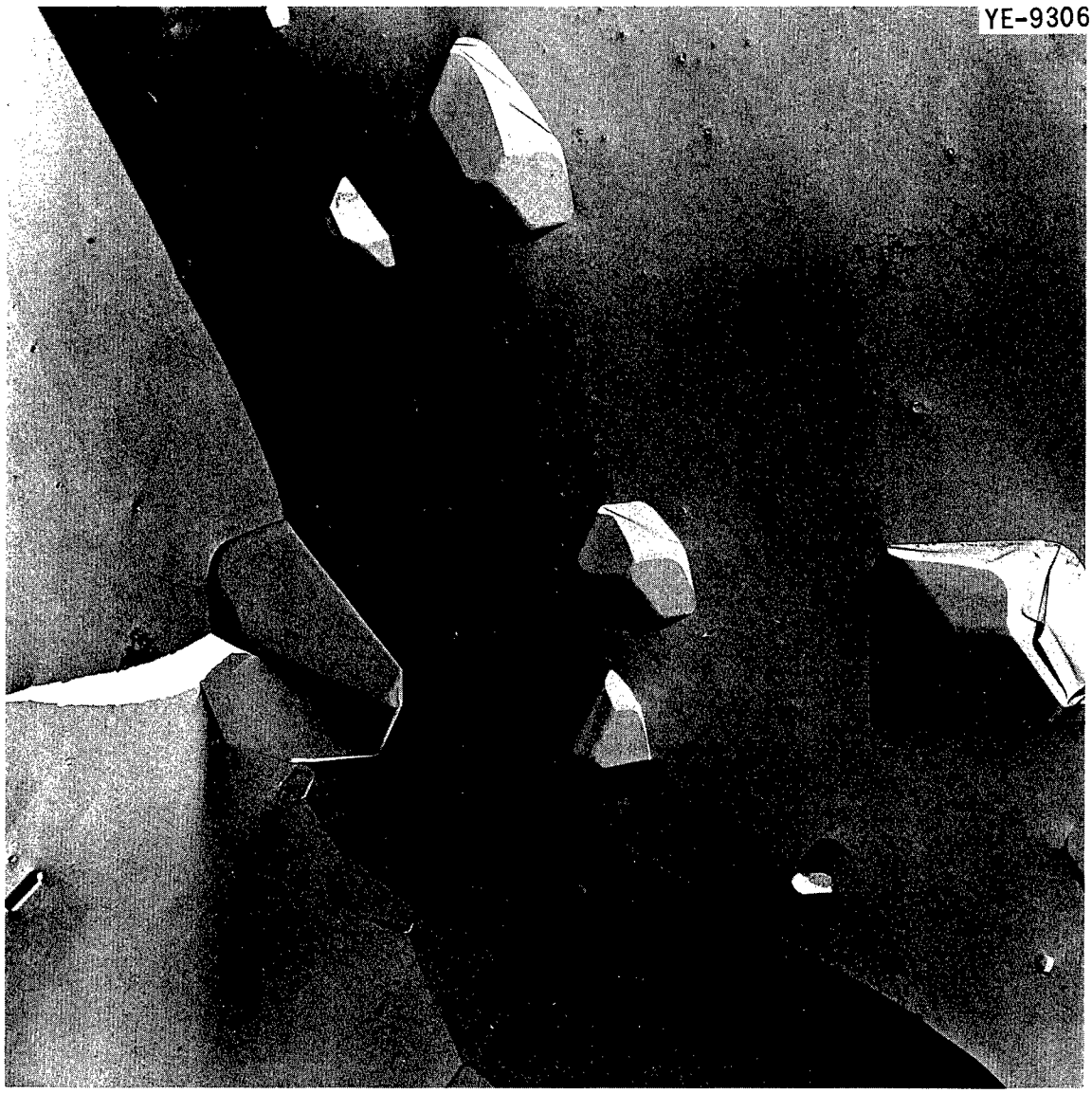

Fig. 7. Fractograph of a PM Tungsten Specimen Tested at 2200°C and 2000 psi. 7500×.

specimens were oriented so that the stress was applied perpendicularly to the columnar grain boundaries.

Figure 9 shows a microstructure typical of lot PW-3 after creep testing at 1650°C. The fracture is intergranular and the cracks are

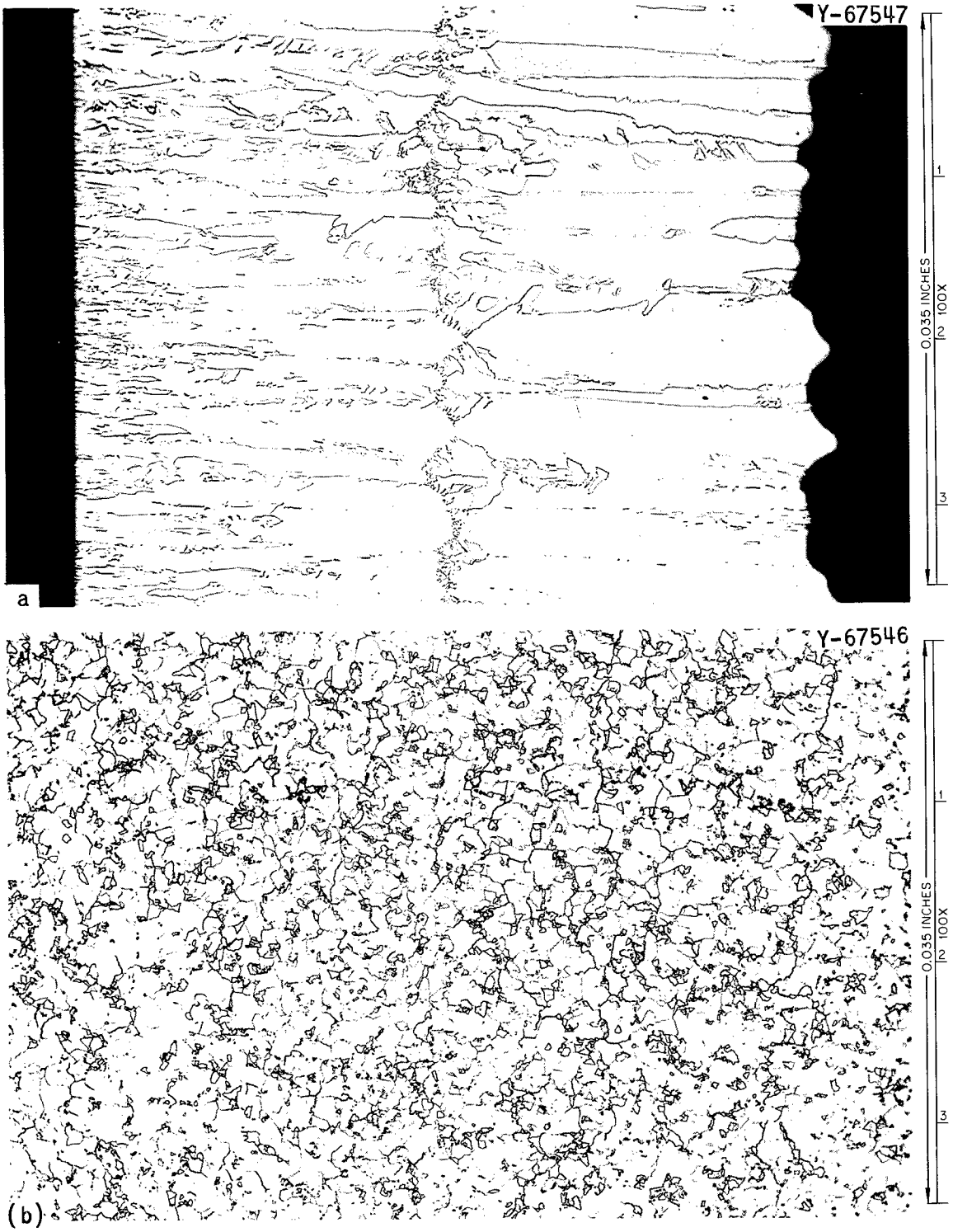

Fig. 8. Photomicrographs of As-Deposited CVD Tungsten, Lot PW-3. Etchant: 50 parts NH_4OH and 50 parts H_2O_2. (a) Cross section. (b) Parallel to surface.

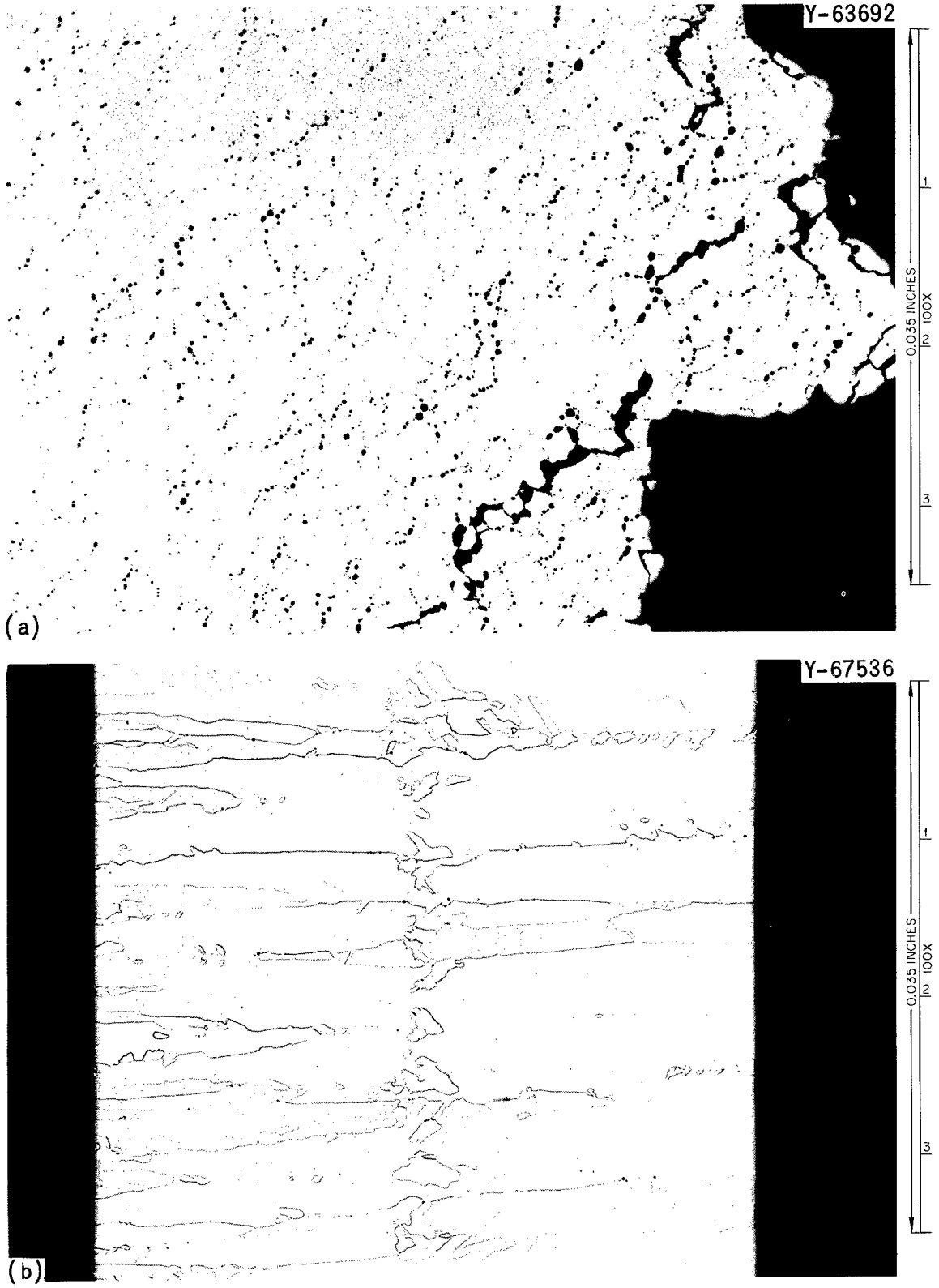

Fig. 9. Photomicrographs of CVD Tungsten from Lot PW-3 Tested at 4000 psi and 1650°C. Failed in 413.0 hr and 3.2% strain. (a) Fracture, as polished. (b) Cross section 1/2 in. from fracture. Etchant: 50 parts NH_4OH and 50 parts H_2O_2.

obviously made up of interconnected voids.[10] The density of voids is reasonably high near the fracture and diminishes rapidly away from the fracture. Figure 10 is a fractograph of a surface about 10 mm from the fracture. Note that the voids present are quite small. Figure 11 is a fractograph made at a similar location in a specimen tested at 1650°C and 6000 psi. By comparison with Fig. 10 it can be seen that the void size is greater at the higher stress, even though this specimen was at temperature a small fraction of the time of the specimen held at the lower stress. The voids in Fig. 11 have very well-defined geometrical shapes as compared with those formed in the PM material under similar conditions (Fig. 5).

Lot H-16 exhibited a somewhat different microstructure, primarily with respect to a greater propensity for void formation. At 1650°C and 6000 psi numerous voids were formed, but the total void fraction was small. At 4000 psi (Fig. 12), the voids were quite large and the void fraction was high. Fractographs showed the presence of large voids with regular, geometrical shapes.

Lot PW-20 also exhibited extensive void formation at 1650°C. Figure 13 shows the fracture of a specimen tested at 6000 psi. The small, almost continuous intergranular network of voids extended throughout the specimen.

We made an effort to increase the fracture ductility at 1650°C by creating a more equiaxial grain structure. This was done by (1) warm work and recrystallization and (2) deposition of a product with a finer grain size. The warm-worked material, lot PW-69, was deformed (by rolling) 80% at 500°C and recrystallized by annealing 1 hr at 2200°C. The specimen, which was then stressed at 6000 psi, failed at a strain of 3.7%. The fracture is shown in Fig. 14. The grain size is large, but the structure

---

[10]We have used the term "void" throughout this paper in referring to the cavities that are formed. In the PM material these cavities are indeed voids. During nucleation and the early stages of growth, the cavities in the CVD material probably contain a gas and are more properly called bubbles. However, under stress these bubbles grow quite large by the condensation of vacancies. The gas pressure likely becomes quite small and the term void is again more descriptive.

Fig. 10. Fractograph Approximately 10 mm from the Fracture of a CVD Tungsten Specimen Tested at 4000 psi and 1650°C. Ruptured in 413 hr with 3.2% strain. 11,250×.

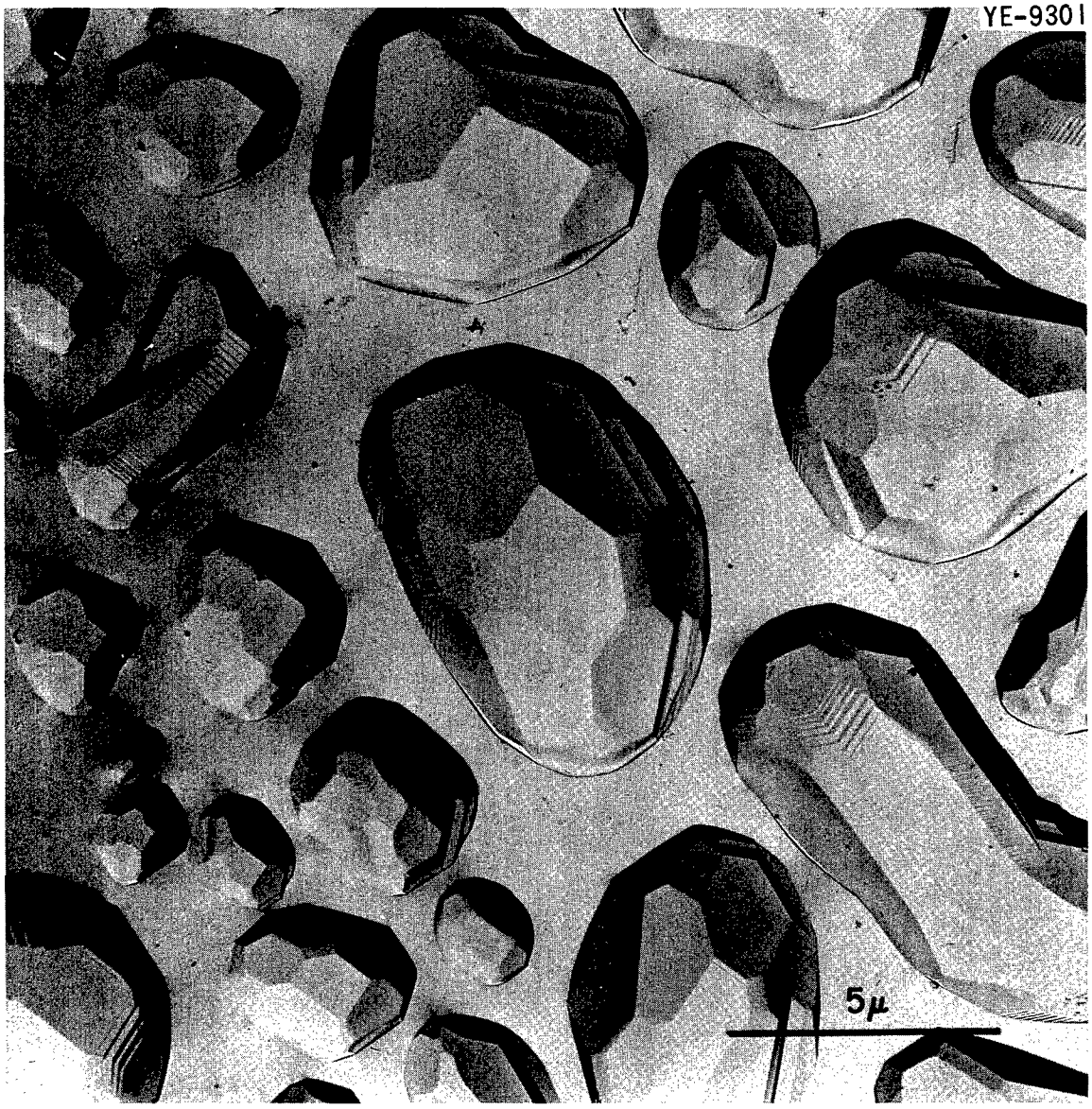

Fig. 11. Fractograph Approximately 10 mm from the Fracture of a CVD Tungsten Specimen Tested at 6000 psi and 1650°C. Ruptured in 12.8 hr with 3.1% strain. 5000×.

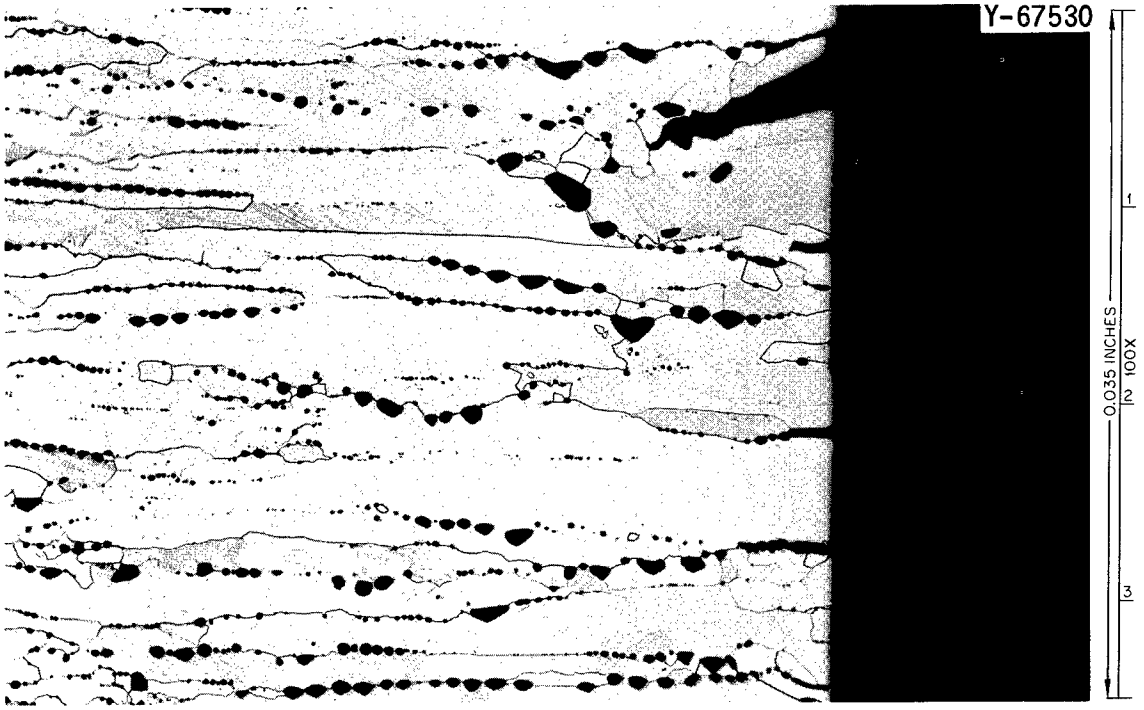

Fig. 12. Photomicrograph of the Cross Section of a CVD Tungsten Specimen from Lot H-16 Tested at 4000 psi and 1650°C. Failed in 593.7 hr with 21.0% strain. Etchant: 50 parts NH_4OH and 50 parts H_2O_2.

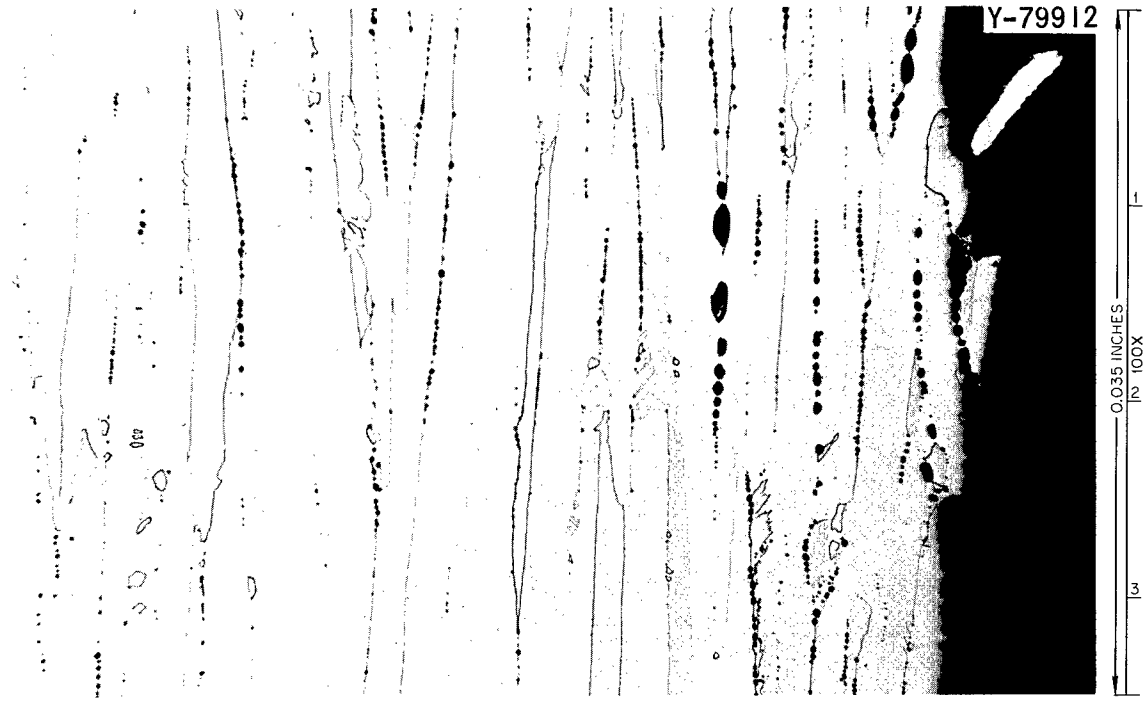

Fig. 13. Fracture of a CVD Tungsten Specimen from Lot PW-20 Tested at 6000 psi and 1650°C. Fractured in 208 hr with 6.3% strain. Etchant: 50 parts NH_4OH and 50 parts H_2O_2.

Fig. 14. Fracture of a CVD Tungsten Specimen from Lot PW-69 Tested at 6000 psi and 1650°C. Warm worked 80% and recrystallized at 2200°C prior to testing. Failed in 37 hr with 3.7% strain. Etchant: 50 parts NH_4OH and 50 parts H_2O_2.

appears equiaxial. The inhomogeneous distribution of the voids is very obvious. The impurity responsible for the nucleation of the voids was probably swept up by the first boundary that moved through each area, thus accounting for the segregation. Figure 15 shows a fractograph of the specimen from lot PW-69. The structure is dominated by the large, crystallographic voids. The material deposited with a finer grain size was lot PW-18. Figure 16 shows the fracture of a specimen from this material that was tested at 1650°C and 6000 psi. A fracture strain of 13.2% was obtained. Although fracture appears to have resulted from the connecting of intergranular voids, there is evidence of considerable plastic deformation. A fractograph of this specimen made on a face about 10 mm from the fracture is shown in Fig. 17. The voids in this specimen resemble more closely those of the PM tungsten (Fig. 5) than

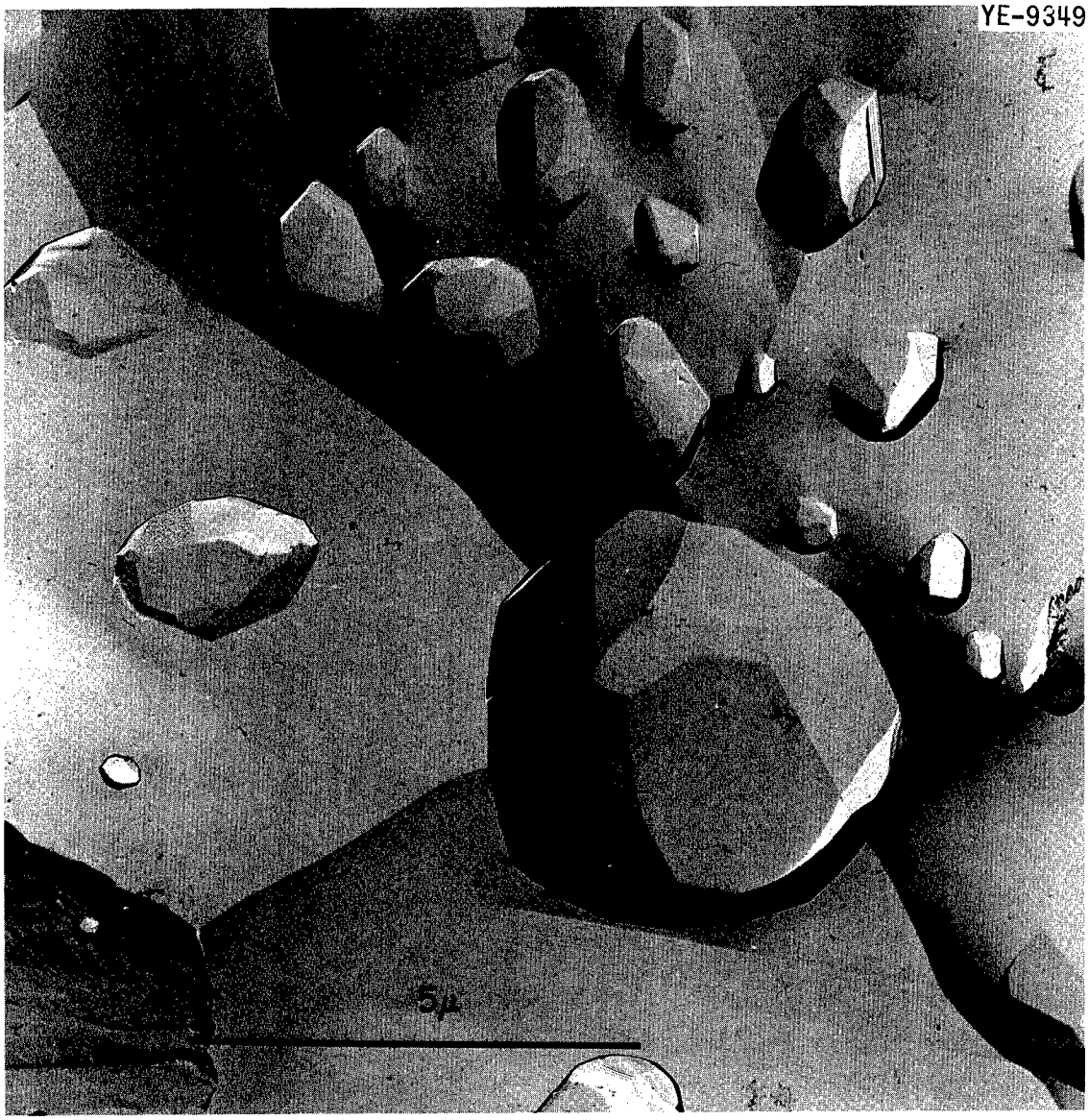

Fig. 15. Fractograph of CVD Tungsten Specimen Approximately 10 mm from Original Fracture. Lot PW-69 tested at 6000 psi and 1650°C. 12,500×.

those of the other CVD specimens. The voids are linking together as well as showing growth in a particular direction.

At 2200°C the various lots of material did not exhibit such a wide variation in microstructural appearance. Figure 18 shows the type of microstructure typically observed for the CVD material that failed in relatively short times. As the stress was lowered and the length of the test increased, the voids were larger and fewer in number (Fig. 19). The

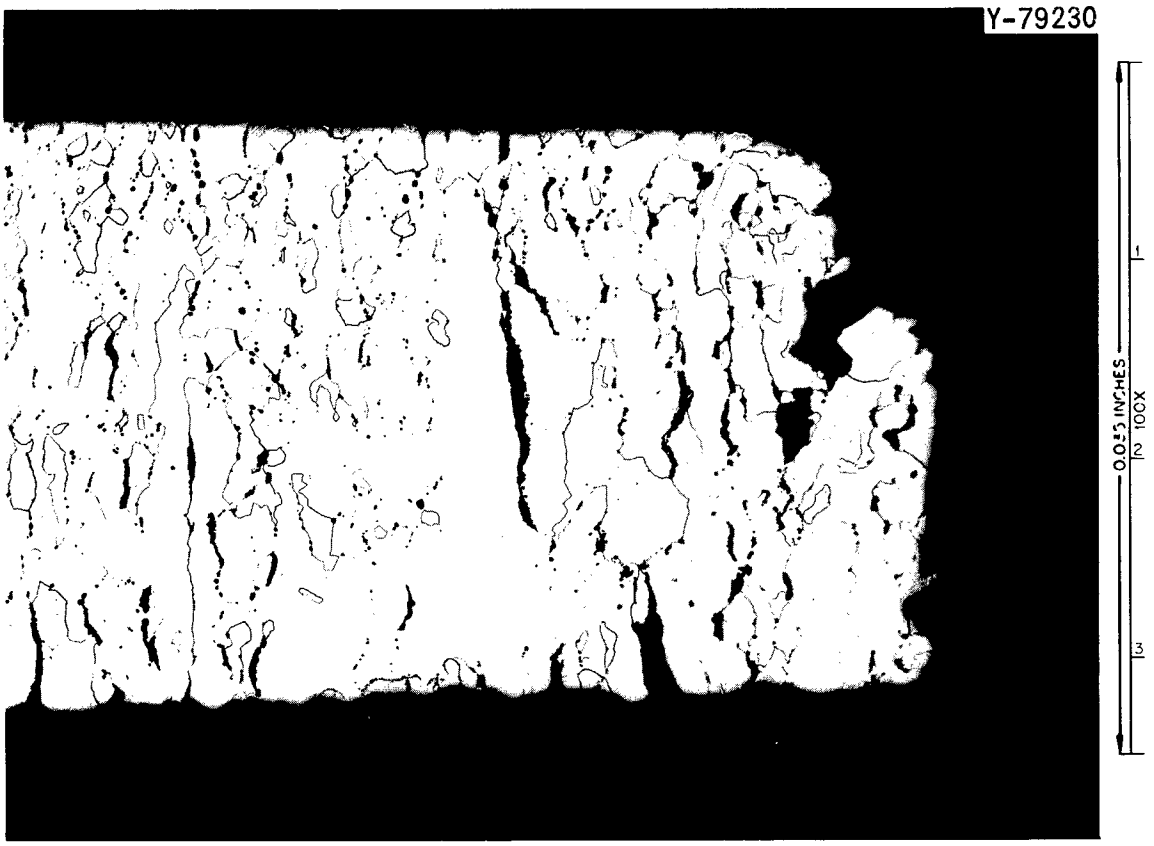

Fig. 16. Micrograph of a CVD Tungsten Specimen from Lot PW-18 Tested at 6000 psi and 1650°C. Failed in 32 hr with 13.2% strain. Etchant: 50 parts NH_4OH and 50 parts H_2O_2.

grain structure also became more equiaxial, indicating the freedom of the boundaries to migrate under stress. The data in Table 3 indicate that the void volume in the specimens from lot PW-3 that were tested at 2200°C did not vary greatly with rupture life. Thus, the larger voids (Fig. 19) were probably formed by the coalescence of the smaller voids (Fig. 18) observed in tests of a shorter duration.

The voids were so large in the specimens tested at 2200°C that they were difficult to study by fractographic techniques. Figure 20 shows an area where the bubbles were relatively small. Note their regular crystallographic shapes. The retention of this regular shape along the boundaries (where three grain surfaces intersect) indicates that very little grain-boundary sliding occurred.

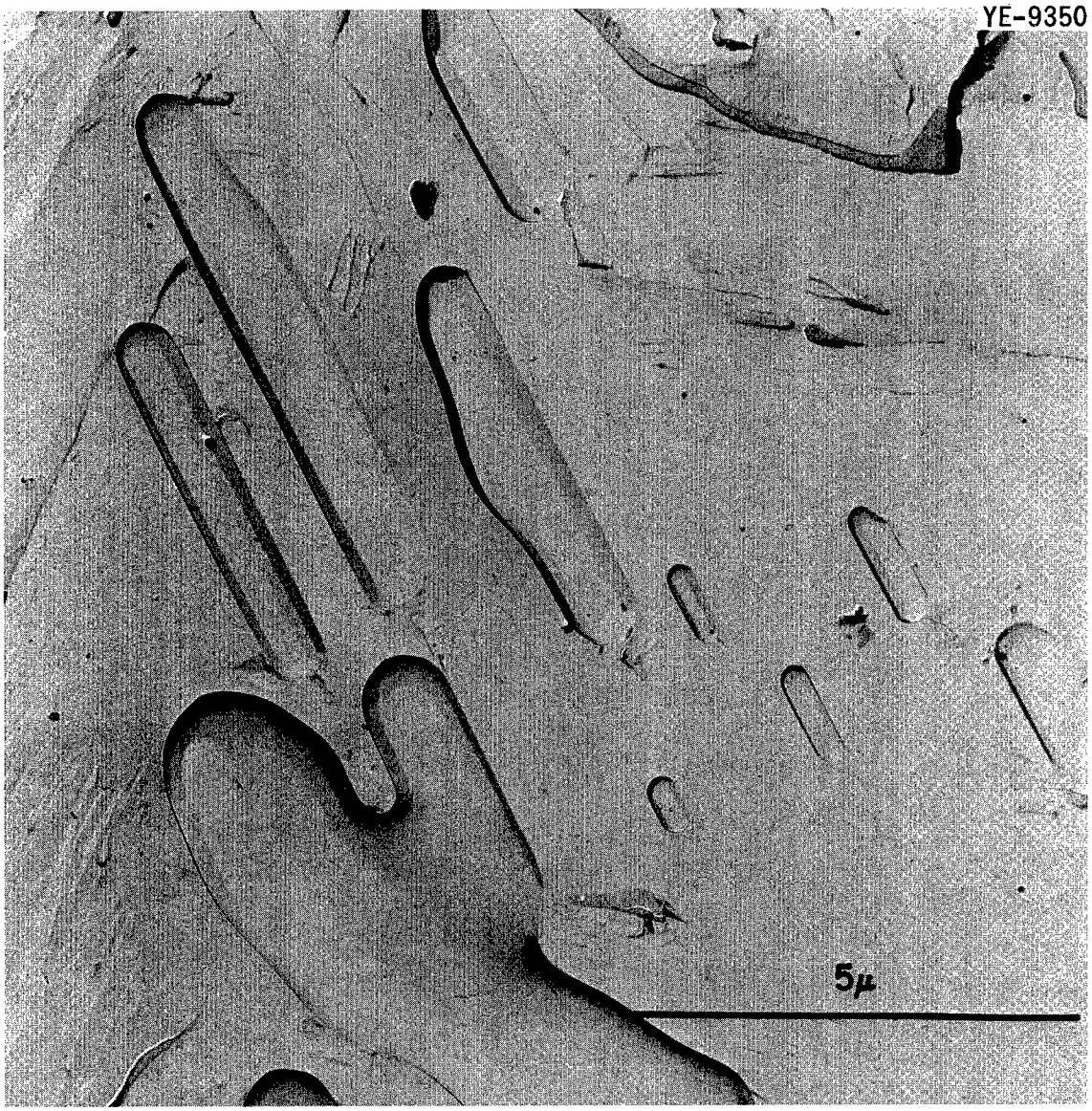

Fig. 17. Fractograph of a CVD Tungsten Specimen Located Approximately 10 mm from Original Fracture Surface. Lot PW-18 tested at 6000 psi and 1650°C. Failed in 32 hr with 13.2% strain. 12,500×.

Although the effect of stress on the growth of voids in the CVD material has been implied in several instances, a comparison of Figs. 18 and 21 clearly demonstrates the effect. These specimens were in the test furnace at the same time, the only difference being that one was unstressed. The void fraction data in Table 3 are again useful. The average void fraction of the stressed specimen was 6.1%, whereas that of the unstressed specimen was only 0.20%.

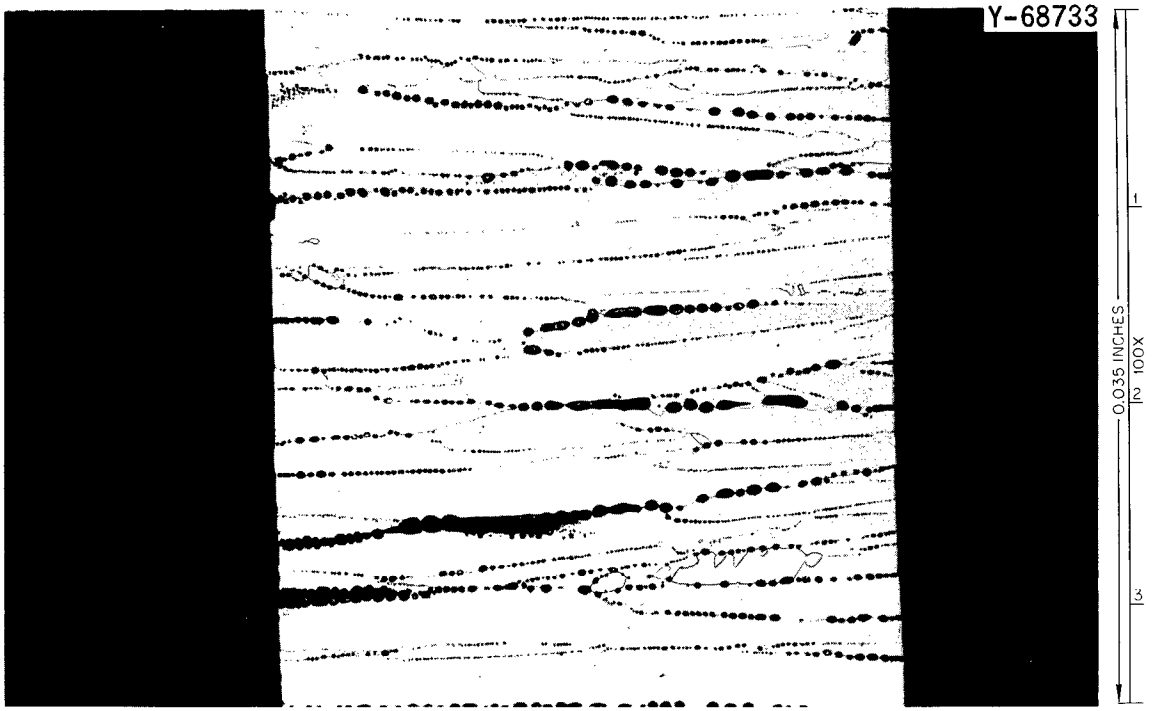

Fig. 18. Cross Section of CVD Tungsten from Lot PW-20 Tested at 2200°C and 2000 psi. Specimen failed at 1.86 hr and 15.6% strain. Etchant: 50 parts NH_4OH and 50 parts H_2O_2.

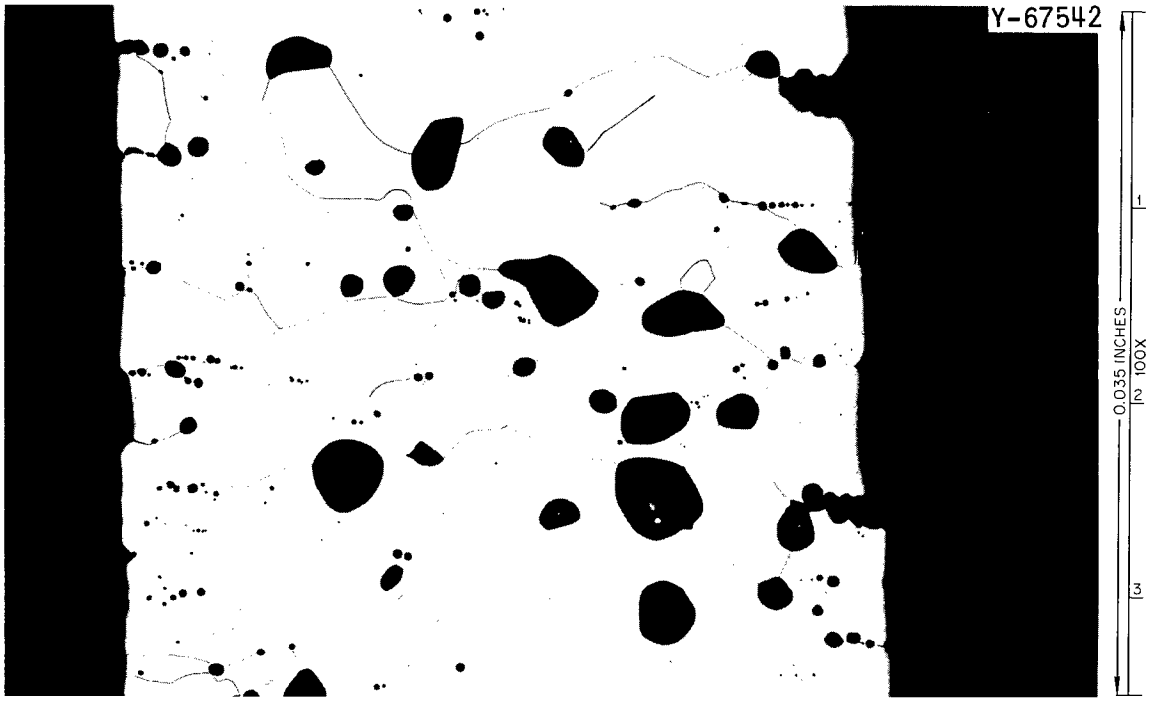

Fig. 19. Cross Section of CVD Tungsten from Lot PW-3 Tested at 2200°C and 2000 psi. Failed at 789.9 hr and 29.2% strain. Etchant: 50 parts NH_4OH and 50 parts H_2O_2.

Table 3. Void Fractions for Various Specimens[a]

Lot Number	Test Conditions	Rupture		Void Fraction, %			Field Size (mm)
		Life (hr)	Strain (%)	Maximum	Minimum	Average	
PW-3	1650°C, 4000 psi	413	3.2	0.35	0.07	0.19	0.43 × 0.31
PW-3	2200°C, 2000 psi	21.3	21.9	11.7	4.5	7.5	0.43 × 0.31
PW-3	2200°C, 1500 psi	35.7	16.6	8.5	4.9	6.9	0.43 × 0.31
PW-3	2200°C, 1250 psi	790	29.2	14.9	4.6	9.1	0.43 × 0.31
PW-20	2200°C, 2000 psi	1.9	15.6	8.1	4.2	6.1	0.43 × 0.31
PW-20	2200°C, 0 psi[b]			0.03	0.50	0.20	0.116 × 0.085

[a]Data by T. M. Kegley, Metallography Group, Metals and Ceramics Division.

[b]Same thermal history as specimen above.

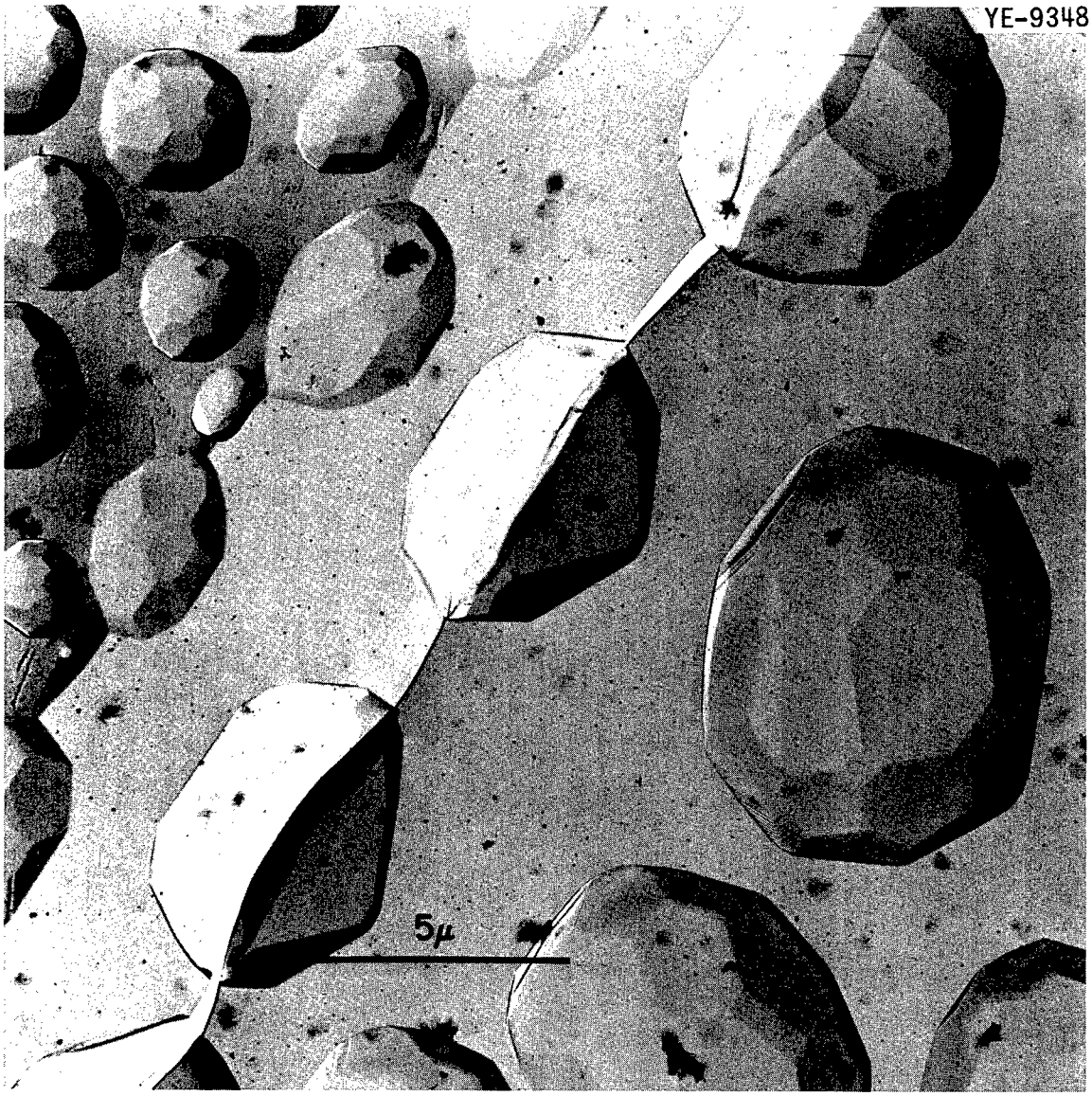

Fig. 20. Fractograph of a CVD Tungsten Specimen from Lot PW-20 Tested at 2000 psi and 2200°C. Located approximately 10 mm from original fracture. Failed in 1.9 hr with 15.6% strain. 7500×.

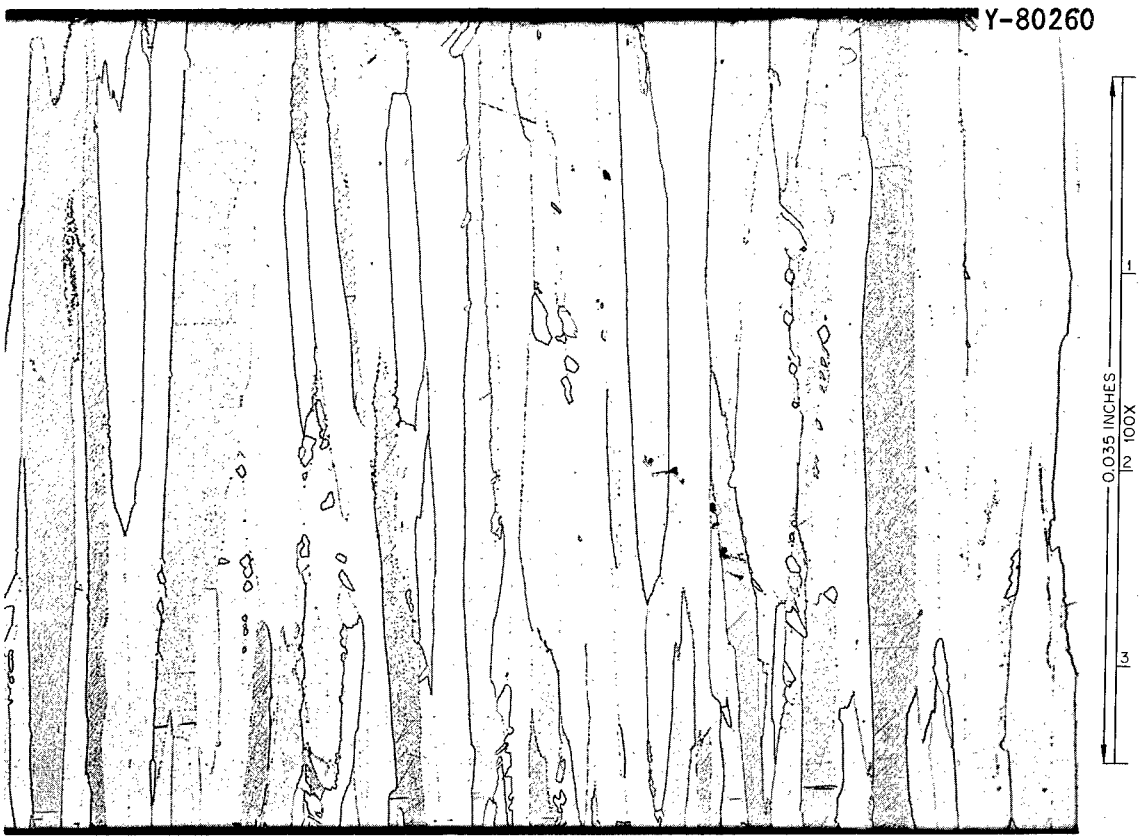

Fig. 21. Photomicrograph of Specimen from Lot PW-20 Annealed 1.9 hr at 2200°C in Vacuum Without Applied Stress. Etchant: 50 parts HN_4OH and 50 parts H_2O_2.

DISCUSSION OF RESULTS

In creep tests at elevated temperatures, void formation or "cavitation" has been observed to lead to intergranular cracking and failure in numerous materials — copper,[11] alpha-brass,[11] magnesium,[11] types 304 and 304L stainless steels,[12] nickel,[13] Inconel 600 (ref. 13), iron,[13] Nimonic 90 (ref. 14), and others. In this work we observed that cracks

[11]J. N. Greenwood, D. R. Miller, and J. W. Suiter, Acta Met. 2, 250 (1954).

[12]Gunji Shinoda, Tadao Sano, and Tadakazu Sakurai, J. Japan Inst. Metals (Sendai) 24, 818 (1960).

[13]H. E. McCoy, Jr., Effects of Hydrogen on the High-Temperature Flow and Fracture Characteristics of Metals, ORNL-3600 (1964).

[14]D. McLean, J. Inst. Metals 85, 468 (1956–57).

developed in both PM and CVD materials from small grain-boundary voids or bubbles although the appearance and behavior of the voids differed in the two types of tungsten. We will now consider how differences in nucleation and growth of such cracks can lead to the differences in structure and properties that were observed.

The several methods that have been proposed for the nucleation of voids have been reviewed by Davies and Dennison.[15] Most mechanisms involve a grain-boundary discontinuity of some type and a shear stress along the boundary. Detailed observations of the PM material suggest that voids were nucleated in this manner as a result of considerable plastic deformation.[16] However, in the CVD material, plastic deformation was not a prerequisite for void formation. Bubbles, formed simply by heating the material to temperatures above about half the absolute melting point, were able to act as void nuclei. The voids (or more properly bubbles) at this stage were likely caused by a locally high concentration of some impurity which is gaseous at the test temperature. The voids (bubbles) are generally attributed to fluorine impurities,[17–19] but the present observations do not show a correlation between the fluorine content and the volume of voids formed under stress. For example, heats H-16 (Fig. 12) and PW-20 (Fig. 13) exhibited a greater propensity for void formation than heat PW-3 (Fig. 9) although the former heats had lower fluorine contents (Table 1). Thus, it appears that, at least under

---

[15]P. W. Davies and J. P. Dennison, J. Inst. Metals 87, 119 (1958–59).

[16]J. O. Stiegler, K. Farrell, B.T.M. Loh, and H. E. McCoy, "Nature of Creep Cavities in Tungsten," submitted to Transactions of the American Society for Metals.

[17]A. C. Schaffhauser and R. L. Heestand, "Effect of Fluorine Impurities on the Grain Stability of Thermochemically Deposited Tungsten," pp. 204–211 in 1966 IEEE Conference Record of the Thermionic Conversion Specialist Conference, Institute of Electrical and Electronics Engineers, New York, 1966.

[18]J. L. Taylor and D. H. Boone, J. Less-Common Metals 6, 157 (1964).

[19]K. Farrell, J. T. Houston, and A. C. Schaffhauser, "The Growth of Grain Boundary Gas Bubbles in Chemically Vapor Deposited Tungsten," paper to be presented at the Conference on Chemical Vapor Deposition of Refractory Metals, Alloys and Compounds, Gatlinburg, Tennessee, September 12–13, 1967.

stress, variables in addition to the bulk fluorine content must be of importance in void formation.

Once nucleated, voids may grow by plastic deformation (dislocation motion and grain-boundary sliding) or by stress-induced vacancy migration and condensation. Under some conditions void growth occurs in the PM material by plastic deformation.[16] However, the limited ductilities of the CVD specimens suggest that plastic processes are not important in determining the rate of growth of the voids. Accordingly, we will consider void growth in the CVD material in terms of the vacancy diffusion process. Any growth by plastic deformation will simply augment the growth by vacancy diffusion.

A void in a solid is thermodynamically unstable and reduction of the surface area of the void by sintering reduces the total energy of the solid. The void can be stabilized by application of a stress to balance the surface tension of the void such that,[20]

$$\sigma = \frac{2\gamma}{r(\cos\ \theta)^2} \qquad (1)$$

where

σ = applied stress,

γ = surface energy of the void,

r = radius of the void,

θ = angle between the normal to the plane in which the void lies and the direction of the applied stress.

If this equality is not met, an elastic strain field surrounding the cavity will either cause it to grow by absorbing vacancies or to shrink by emitting them. If a gas is present in the void, the applied stress necessary to stabilize a void of a given radius will be reduced.

The problem in calculating the vacancy flux into a void lies in estimating the elastic strain field surrounding the void. This determines

---

[20]R. W. Balluffi and L. L. Seigle, Acta Met. 5, 449 (1957).

the chemical potential of a vacancy in the vicinity of the void. Hull and Rimmer[21] simplified the problem by assuming that the potential varied linearly from a value of $-\frac{2\gamma\Omega}{r}$ on the surface of the void to a value $\sigma\Omega$ at a point midway between voids, where Ω is the atomic volume and σ is the tensile stress normal to the void. On this basis they showed that the vacancy flux into the void, j, was given approximately by:

$$j \cong \frac{D_g}{kTa}\left[\sigma + P - \frac{2\gamma}{r}\right], \qquad (2)$$

where

D_g = grain-boundary diffusion coefficient,
k = Boltzmann's constant,
T = absolute temperature,
a = void spacing,
P = gas pressure inside void.

This expression shows that the growth rate is proportional to the difference between (1) the sum of the applied stress and the pressure in the bubble and (2) a term proportional to the surface tension of the bubble. Temperature enters mainly through the exponential dependence of D_g on temperature.

When CVD material is heated to temperatures above about 1400°C, a gaseous phase precipitates, forming bubbles having a range of sizes.[19] If a stress is applied, the vacancy flux into the bubble is approximated by Eq. (2). Small bubbles will grow until they reach an equilibrium size at which time j equals 0. For bubbles larger than some critical size, r_c, equilibrium cannot be established and these bubbles will continue to grow indefinitely. In terms of Eq. (2), r must decrease to reach equilibrium, but the sign of j is such to cause r to increase.

We can now understand the differences in creep behavior between the CVD and PM materials in terms of nucleation and growth of voids. In the PM material no void nuclei were present initially; voids were nucleated by plastic deformation. In the CVD material the grain boundaries were

---

[21]D. Hull and D. E. Rimmer, Phil. Mag. 4, 673 (1959).

covered with bubbles which acted as void nuclei. At high stresses, many of these bubbles were larger than the critical size. They grew and linked up, causing failure in a short time. At lower stresses, fewer nuclei of the critical size were present, their growth rate was lower, and longer rupture times resulted. This explanation accounts for the decreased rupture times at the higher stresses for CVD specimens and for the decreased slope of the stress-rupture time curve. It also suggests that, for sufficiently low stresses, bubble growth cannot occur and that the stress-rupture curves of the CVD and PM materials will intersect. For reasons to be discussed below, we feel that extensive grain-boundary sliding does not occur in CVD material. Since cavities in the PM material are believed to result from sliding, it is possible that the creep-rupture curves cross and at sufficiently low stresses the CVD material may have longer rupture lives.

The question of fracture ductility is more complex, for we must consider not only growth of voids and the elongation they provide, but also the concomitant processes of grain-boundary sliding and bulk deformation. The total strain, ϵ_T, is the sum of the contributions from bulk deformation, ϵ_g, grain-boundary sliding, ϵ_b, and void formation, ϵ_v. The bulk strain arises mainly from dislocation motion. Since the purities of the PM and CVD materials were comparable, they should show roughly equivalent bulk strain contributions.

Garofalo[22] has recently reviewed the data on grain-boundary sliding. In general, the strain contribution from grain-boundary sliding increases as the stress decreases and as the temperature increases. Grain-boundary sliding requires a shear stress along the grain boundary. Such a stress was probably present in the PM specimens, as evidenced by the elongated shapes of the voids. Such shapes could result from plastic deformation or from stresses that would produce vacancy flux gradients favorable for this type of growth. However, the magnitude of the strain in PM tungsten due to grain-boundary shearing at 2200°C probably decreased rapidly with time due to the excessive grain growth. The CVD tungsten had two factors

[22]Frank Garofalo, p. 142 in Fundamentals of Creep and Creep-Rupture in Metals, Macmillan, New York, 1965.

that combined to reduce ϵ_b to negligible values. The first was the void formation that occurred. Shearing the voids would produce some new surface area and thus would require a greater stress than if the voids were not present. There may also be a strain field associated with the voids since some localized plastic deformation could have occurred during the nucleation and early growth of the void. Only lot PW-18 showed any evidence of grain-boundary deformation (Fig. 17). A second and probably more important factor was the columnar grain structure of the CVD material. The microstructure of the deposits approaches that of long rods packed together with their axes perpendicular to the applied stress. It would seem difficult to develop shear stresses of sufficient magnitude to cause grain-boundary sliding since no shearing stress could be developed parallel to the axis of the rod. Although there would be a shearing stress tending to rotate the rods, such a movement would involve much material and would require very high stresses. Thus, some semblance of an equiaxial grain structure would appear to be necessary for extensive grain-boundary sliding to occur. This was only obtained (1) after long periods of time at 2200°C where some grain-boundary migration could occur (Fig. 19), (2) in lot PW-69 which was worked and recrystallized (Fig. 14), and (3) in lot PW-18 which was deposited with a fine-grain structure (Fig. 16).

It is significant that lot PW-18 exhibited good ductility at 1650°C. The fine-grain size of this material may be due to the cadmium impurity present. Although the fluorine content was lower than that of the other heats, there was still profuse bubble formation. Hence, we feel that the improved ductility of this material was due primarily to the change in the grain structure. However, we must point out that these two factors, grain structure and fluorine content, may not be entirely independent in the CVD material. For example, previous studies have shown that greater grain-boundary mobility is obtained with decreasing fluorine content.[17] Thus, the lower fluorine content would allow grain-boundary migration to occur with the resultant formation of a more equiaxial structure that would be more conducive to grain-boundary shearing and rotation. However, it remains to be demonstrated whether under stress the threshold fluorine (or other impurity) levels are high enough to be attained in practice.

Before stressing, lot PW-69 was heated to 2200°C for recrystallization with attendant large void formation. There was no evidence of grain-boundary sliding in this material. Thus we would conclude that the ϵ_b would be very small at 1650°C, except in lot PW-18, and would probably be small at 2200°C except after long test periods.

The grain-boundary sliding process is important not only because of its contribution to the overall strain but because it acts as a stress-relieving mechanism. The deformation of individual grains leads to large local stresses that can be relieved by sliding. Hence, in the absence of sliding, these stresses may lead to cracking between the intergranular voids with resultant premature failure.

The strain due to the voids is most significant at 2200°C. Table 3 lists the results of some void fraction measurements made on the test specimens. At 1650°C the strain due to void formation in lot PW-3 was a maximum of 0.35%. However, the strain due to void formation was higher in lots PW-20 (Fig. 13) and H-16 (Fig. 12). At 2200°C lot PW-3 had void fractions of 7 to 9%. There was no measurable reduction in width of the specimen, and the total void fraction can be assumed to be axial strain. The other lots of material exhibited similar void growth at 2200°C and we can conclude that up to 10% of the strain in this material can be attributed to void growth.

The creep properties shown in Figs. 1, 2, and 3 can be rationalized by the way that the various terms contributing to the total strain are affected — ϵ_g, ϵ_b, and ϵ_v. At 1650°C, ϵ_b and ϵ_v are both generally low at high stresses. The creep rate is lower, but the inability for boundary deformation to occur leads to reduced ductility and slightly reduced rupture life. At low stresses (approx 4000 psi) the stress is not high enough for extensive void growth to occur (Fig. 10). Thus, the rupture time more closely approaches that of the PM material. However, the material still lacks the ability to undergo extensive grain-boundary sliding with resultant low minimum creep rate and low fracture strain.

The high strain of sample H-16 at 4000 psi was due to the extensive void formation and a large value of ϵ_v. Lot PW-18 also differed in that the more equiaxial structure resulted in a relatively large value of ϵ_b.

The result was a higher creep rate and rupture strain. At 2200°C the ϵ_b term is probably initially small and ϵ_v is large. This results in higher creep rates, high apparent ductilities, and generally lower rupture lives.

CONCLUSIONS

We have compared the creep-rupture results of several lots of CVD tungsten with those of PM tungsten. The failed PM tungsten specimens contained intergranular voids that linked together to form intergranular cracks. The CVD tungsten formed voids simply on heating to elevated temperatures. These voids grew under the influence of an imposed stress. The presence of these intergranular voids and the columnar grain structure of the CVD material combined to reduce the amount of grain-boundary shearing that occurred. At 1650°C the minimum creep rate and the rupture ductility of the CVD tungsten were less than those of the PM tungsten. The rupture life of the CVD tungsten was less at higher stresses and equivalent at lower stresses. The stabilization of more voids and their subsequent growth at the higher stress are thought to be responsible for the rupture behavior. The lower creep rate and ductility were due to the inability for grain-boundary shearing to occur. One lot of material that had a fine-grain size exhibited much better fracture ductility.

At 2200°C the voids were so large that they contributed significantly to the measured strain. The minimum creep rate was higher and the rupture life was lower for this material than for PM tungsten.

ACKNOWLEDGMENTS

The authors are indebted to several persons and groups who contributed to this study: E. Bolling and B. McNabb, for running the creep-rupture tests; H. R. Tinch, for the optical metallography; Metals and Ceramics Division Reports Office, for the preparation of the manuscript; D. G. Gates, for the drawings; ORNL Analytical Chemistry Division, for the chemical analyses; E. E. Bloom and A. C. Schaffhauser, for the technical review of the manuscript.

ORNL-4162
UC-25 — Metals, Ceramics, and Materials

INTERNAL DISTRIBUTION

1–3. Central Research Library
4–5. ORNL — Y-12 Technical Library Document Reference Section
6–25. Laboratory Records Department
26. Laboratory Records, R.C.
27. ORNL Patent Office
28. E. G. Bohlmann
29. G. E. Boyd
30. J. A. Conlin
31. G. L. Copeland
32. R. S. Crouse
33. J. E. Cunningham
34. J. H. DeVan
35. R. G. Donnelly
36. J. I. Federer
37. D. E. Ferguson
38. B. Fleischer
39. M. H. Fontana
40. J. H Frye, Jr.
41. R. E. Gehlbach
42. W. O. Harms
43–46. M. R. Hill
47. G. W. Keilholtz
48. R. T. King
49. C. E. Larson
50. D. J. Legacy
51. A. Litman
52. B. T. Loh
53. H. G. MacPherson
54. W. R. Martin
55–64. H. E. McCoy, Jr.
65. D. L. McElroy
66. S. E. Moore
67. J. P. Moore
68. G. T. Newman
69. A. C. Schaffhauser
70. C. E. Sessions
71. J. E. Simpkins
72. G. M. Slaughter
73. R. L. Stephenson
74. J. O. Stiegler
75. S. C. Weaver
76. A. M. Weinberg
77. J. R. Weir
78. R. P. Wichner
79. R. E. Worsham
80. G. T. Yahr
81. M. B. Bever (consultant)
82. A. R. Kaufmann (consultant)
83. J. A. Krumhansl (consultant)

EXTERNAL DISTRIBUTION

84. G. M. Anderson, AEC, Washington
85. C. H. Armbruster, Wright-Patterson AFB
86–88. V. P. Calkins, General Electric, NMPO
89. S. S. Christopher, Combustion Engineering, Inc.
90. D. F. Cope, RDT, SSR, AEC, Oak Ridge National Laboratory
91. J.W.R. Creagh, NASA, Lewis Research Center
92. J. Davis, Jet Propulsion Laboratory
93. R. W. Dayton, Battelle Memorial Institute
94. G. K. Dicker, AEC, Washington
95. E. M. Douthett, AEC, Washington
96. J. K. Elbaum, Code MAMP, Wright-Patterson AFB
97. D. DeHalas, Pacific Northwest Laboratory, Richland
98. D. C. Goldberg, Westinghouse Astronuclear Laboratory
99. J. L. Gregg, Bard Hall, Cornell University

100–101. D. H. Gurinsky, Brookhaven National Laboratory
102. R. Hall, NASA, Lewis Research Center
103. R. C. Hamilton, Institute for Defense Analyses, 1666 Connecticut Avenue, N.W., Washington, D.C.
104. E. E. Hoffman, General Electric, Cincinnati
105. W. R. Holman, Lawrence Radiation Laboratory
106. C. Johnson, Space Nuclear Systems Division, Space Electric Power Office, AEC, Washington, D.C. 20545
107. J. S. Kane, University of California
108. W. J. Larkin, AEC, Oak Ridge Operations
109. J. J. Lombardo, NASA, Lewis Research Center
110. J. J. Lynch, NASA, Washington
111. T. P. Moffitt, NASA, Lewis Research Center
112–114. T. A. Moss, NASA, Lewis Research Center
115. R. A. Noland, Argonne National Laboratory
116. Louis Rosenblum, NASA, Lewis Research Center
117. A. J. Rothman, Lawrence Radiation Laboratory
118. B. Rubin, Lawrence Radiation Laboratory
119. N. D. Sanders, NASA, Lewis Research Center
120. H. Schwartz, NASA, Lewis Research Center
121. F. C. Schwenk, AEC, Washington
122–126. J. M. Simmons, AEC, Washington
127. D. K. Stevens, AEC, Washington
128. J. A. Swartout, Union Carbide Corp., New York
129. G. W. Wensch, AEC, Washington
130. M. J. Whitman, AEC, Washington
131. Research and Development Division, AEC, Oak Ridge Operations
132–403. Given Distribution as shown in TID-4500 under Metals, Ceramics, and Materials Category (25 copies – CFSTI)